Amplitude-Mode Spectroscopy of Charge Excitations in PTB7 π-Conjugated Donor-Acceptor Copolymer for Photovoltaic Applications

Sangita Baniya, Shai R. Vardeny, Evan Lafalce, Nasser Peygambarian, and Z. Valy Vardeny

Phys. Rev. Applied **7**, 064031 — Published 28 June 2017

DOI: 10.1103/PhysRevApplied.7.064031

Amplitude Modes Spectroscopy of Charge Excitations in PTB7 π-Conjugated Donor-Acceptor Copolymer for Photovoltaic Applications

Sangita Baniya[1†], Shai R. Vardeny[2†], Evan Lafalce[1], Nasser Peygambarian[2] and Z. Valy Vardeny[1]*

[1] *Department of Physics & Astronomy, University of Utah, Salt Lake City, Utah 84112, USA*

[2] *College of Optical Sciences, University of Arizona, Tucson, Arizona 85721, USA*

Abstract

We measured the spectra of resonant Raman scattering and doping induced absorption of pristine films of the π-conjugated donor-acceptor (D-A) copolymer, namely Thieno[3,4 b]thiophene-alt-benzodithiophene (PTB7), as well as photoinduced absorption spectrum in blend of PTB7 with fullerene PCBM molecules used for organic photovoltaic (OPV) applications. We found that the D-A copolymer contains six strongly coupled vibrational modes having relatively strong Raman scattering intensity, which are renormalized upon adding charge polarons onto the copolymer chains either by doping or photogeneration. Since the lower energy charge polaron absorption band overlaps with the renormalized vibrational modes, they appear as anti-resonance lines superposed onto the induced polaron absorption band in the photo-induced absorption spectrum, but less so in the doping induced absorption spectrum. We show that the Raman scattering, doping- and photoinduced absorption spectra of PTB7 are well explained by the amplitude mode model, where a single vibrational propagator describes the renormalized modes and their related intensities in detail. From the relative strengths of the induced infrared activity of the polaron-related vibrations and electronic transitions we obtained the polaron effective kinetic mass in PTB7 using the amplitude mode model to be ~3.8m^*, where m^* is the electron effective mass. The enhanced polaronic mass in PTB7 may limit the charge mobility, which, in turn reduces the OPV solar cell efficiency based on PTB7/fullerene blend.

† These authors contributed equally to this work.

*Corresponding author; e-mail address: val@physics.utah.edu

Introduction

Organic photovoltaics (OPVs) based on blend films of organic semiconductors such as π-conjugated polymers and fullerene molecules have attracted significant interest as a potential lightweight, low-cost renewable energy source [1-5]. The donor polymer materials were homopolymers such as polythiophene that absorb in the visible range of the solar spectrum [6]. However, homopolymers have recently been replaced by block copolymers whose repeat units consist of alternating donor (D) and acceptor (A) moieties [7-16]. This chain architecture reduces the optical gap drastically, and thus the D-A copolymers absorb in the near infrared, where the largest fraction of the photons emitted by the Sun lies. The power conversion efficiencies (PCE) of organic solar cells with D-A copolymers as donor materials and fullerene molecules as acceptors have exceeded 10% [16], approaching the 12% threshold for commercial viability [2,17]. Despite the increasing interest in device applications, there is only limited understanding of the molecular doping of D-A conjugated copolymers [18], or the nature and properties of the charge excitations (polarons) in these materials [19-27]. This requires deeper understanding of the vibrational modes associated with the polaron excitation in the D-A copolymer chains since the strongly coupled vibrations may enhance the polaron mass thereby inhibiting its mobility.

The polaron excitation in π-conjugated polymers distorts the chain dimerization pattern and this renormalizes the strongly coupled vibrations [28]. Consequently, Raman active modes having even parity character (i.e. A_g symmetry modes) become infrared active with very large oscillation strengths [29]. These modes, dubbed infrared active vibrations (IRAVs) appear upon doping or charge photogeneration and are thus signature of charges added onto the polymer chain [30, 31]. One way to describe the IRAVs in π-conjugated polymers is via the amplitude mode model (AMM) that was successfully advanced by Horovitz and collaborators for polyacetylene, $(CH)_x$ [29,30]. The AMM has had enormous success in describing the vibrations of the ground and excited states of trans- and cis-$(CH)_x$. In addition, it has also been used to analyze the strong dispersion of the Raman modes with the laser excitation frequency in t-$(CH)_x$ as measured by resonant Raman scattering (RRS) spectroscopy [29,30,32]. The IRAVs in this and other polymers appear in the absorption spectrum as intense absorption lines if the absorption bands of the charge polaron do not overlap with the vibrational modes. However,

when the charge polaron lower absorption band overlap with the vibrational modes then quantum interference between the two features may occur in the form of multiple Fano effect, where the IRAVs manifest themselves in the form of anti-resonances (ARs) superimposed on the polaron lower absorption band [28, 33]. Since the lower polaron absorption band in low bandgap D-A copolymers should be in resonance with the IRAVs, it is expected that ARs would dominate the absorption spectrum when charges are added to the copolymer chains. Yet the anticipated ARs have not been studied in D-A copolymers, and the suitability of the AMM to describe the vibrational modes in these compounds has not been validated. Therefore, important information on the charge polarons in these copolymers could not be obtained.

To achieve p-type molecular doping in π-conjugated polymers, highly electronegative molecules are mixed in low concentration with the organic chains [18]. Here we focus on p-type doping, namely the introduction of excess positive polarons into the copolymer chains. The most commonly accepted picture is the ground-state transfer of one electron from the highest occupied molecular orbital (HOMO) of the polymer to the lowest unoccupied molecular orbital (LUMO) of the electronegative dopant molecule, thereby enhancing the polymer film conductivity. However, recent observations show evidence that the effect of doping on conductivity enhancement in D-A copolymers is lower than that for homopolymers [18]. It is thus interesting whether the inability of p-type doping is a common property for the π-conjugated copolymers that are used in OPV applications.

For our investigations we have chosen the D-A copolymer thieno[3,4-b]thiophenealt-benzodithiophene (PTB7); see structure in Fig. 1(a) [34]. PTB7 is a low band-gap copolymer with optical gap in the near-IR spectral range, namely at ~ 1.7 eV (Fig. 1(b)) [34,35]. When blended with PCBM, the PTB7 blend has achieved photovoltaic PCE of up to 9% in an optimized device architecture [35]. Alas a recent study demonstrated that PTB7 degrades under accelerated conditions, showing a rapid loss of absorption compared to homopolymers such as P3HT and PPV [36,37]. To characterize the strongly coupled vibrational modes of the copolymer that influence the polaronic mass we measured the RRS, doping-induced absorption (DIA) and photoinduced absorption (PIA) spectra in films of pristine PTB7 and PTB7/PCBM blend, respectively. We show that the main charge excitation of the PTB7 chains is the polaron having

two characteristic absorption bands below the gap [25]. Since the low-energy polaron absorption band indeed overlaps with the strongly coupled vibrational modes, these modes mostly appear in the DIA and PIA spectra as ARs superimposed on the polaron absorption band. Nevertheless, we show that the AMM can still provide an excellent basis for understanding the various vibrational spectra, since it describes all three spectra in detail. Using the AMM parameters and the relative strengths of the IRAVs compared to the polaron absorption bands, we calculate the polaron effective mass in PTB7 to be ~3.8m*, where m* is the effective electron mass in this copolymer chain [25]. The polaronic mass enhancement may inhibit the charge mobility in this compound, which, in turn may reduce the obtained OPV solar cell efficiency.

Experimental

The PTB7 copolymer powder was purchased from Solarmer and used without further purification. Thin films of PTB7 were spin cast or drop cast from PTB7 solution in 1,2-Dichlorobenzene (ODCB) at concentration of 10 mg/ml onto sapphire or KBr substrates, depending on the spectral range of interest. For the PTB7/PCBM blend we used a solution of PTB7 and $PC_{60}BM$ (1:1.5 in weight) with the same concentration in ODCB, which was stirred in Nitrogen atmosphere overnight. The sample films were placed in a cryostat equipped with transparent windows in the visible to mid-IR, where the temperature could be regulated between 40-300K.

The photoluminescence (PL) and absorption spectra of the pristine films were measured using a steady state photomodulation pump-probe setup [38], where the pump was a diode laser at 486 nm and intensity of ~ 100 mW/cm^2. For PIA, the probe beam was derived from an incandescent Tungsten lamp (visible spectral range) or glow-bar (mid-IR range) and passed through a ¼ met monochromator optimized at various wavelengths throughout the visible, near-IR and mid-IR spectral ranges. A variety of semiconductor detectors such as Si, Ge and InSb were used to monitor the transmission, T through the sample film, and the changes, ΔT induced by the pump beam. The PIA spectrum was subsequently calculated as $-\Delta T/T$. To cover the spectral range of 500-4000 cm^{-1} we used an FTIR spectrometer. For obtaining the PIA spectrum, we used a shutter to modulate the laser illumination on the film, and we signal-averaged the IR absorption

spectrum for 6000 scans [33]. For the DIA spectrum, we doped the film p-type by exposing it to iodine vapor for various time durations ranging from a few seconds to one hour. The Raman scattering spectrum was measured using a micro-Raman spectrometer equipped with a cw laser at 486 nm where the inelastic scattered light was detected with a filter and a photomultiplier tube.

Results and Discussion

Figure 1 shows the absorption and PL spectra of pristine PTB7 film. Figure 1(a) shows the copolymer backbone repeat unit; the repeat unit is composed of donor and acceptor moieties [34]. In Fig. 1(b) it is seen that the absorption onset is at 1.7 eV, whereas the absorption peaks at ~ 1.8 eV with the maximum slope at 1.75 eV; this is the mean exciton energy in PTB7. One of the reasons for the low optical gap here is the difference in electron affinity between the donor and acceptor moieties in the copolymer chain [27]. The absorption spectrum shows a second pronounced band ~150 meV higher than the first band, which we consider to be a 'vibration replica'. We note that a third band occurs in the absorption spectrum at ~ 3.1 eV, which may be due to a second transition of the copolymer chain [39,40].

The PL spectrum shown in Fig. 1(b) is composed of two pronounced bands that are in the form of 'mirror image' of the absorption spectrum close to the band-edge, that are ~150 meV apart. The PL main peak is at 1.55 eV having an apparent 'Stokes shift' of ~ 250 meV from the main absorption peak. However, this large energy difference is mainly caused by exciton diffusion to sites on the chain that have the lowest energy, rather than a natural, intrinsic Stokes shift. The relatively low optical gap of PTB7 makes it attractive for organic photovoltaic applications [34, 39].

The expected difference in electron affinity of the donor and acceptor moieties raises the question whether the inversion symmetry is broken in this copolymer chains [27]. This can be checked by Raman scattering and IR-absorption. If the chain inversion symmetry still holds, then the Raman active vibrations are not IR-active, and vice versa. Figure 2 shows the RRS spectrum compared to the IR-absorption spectrum in pristine PTB7 film on KBr substrate. The RRS spectrum contains six strongly coupled modes that are labeled 1-6 (Fig. 2(a)). We note that the

two modes above 1600 cm^{-1} have been identified as due to impurities and defects on the chains [37], and thus we do not analyze them in detail. It is interesting to note that the C=C stretching mode in PTB7 shows a group of Raman-active modes stretching from 1400 to 1600 cm^{-1}. This is probably caused by a distribution of the C=C frequency due to the different environments on the copolymer chain close to the donor, acceptor and the 'in between D-A' place [37]. On the contrary, the IR absorption spectrum shown in Fig. 2(b) contains many more IR-active modes than in the RRS spectrum; and there is no resemblance of the two spectra. We therefore conclude that the copolymer chain approximately retains the inversion symmetry operation.

Figure 3 shows the evolution of the IR-absorption spectrum in PTB7 upon iodine doping for various durations. We note that doping of PTB7 has occurred relatively easy here, similar to doping of many homopolar polymers; and in contrast to other copolymers discussed in the literature [18]. We can divide the DIA spectrum in PTB7 into two regions; namely the vibrational spectral range up to ~1500 cm^{-1} and the electronic range at higher photon energy. The absorption strength in both ranges intensifies similarly with the iodine exposure time, showing that they are correlated. The absorption increase also shows that both ranges lure their oscillator strength from the ground state absorption due to charges that are added onto the chains by the iodine molecule dopants. We identify the strong vibrations as IRAVs showing that the added charges onto the copolymer chains give rise to new IR-active vibrations in agreement with the extra charges [30]. It is rather surprising that the IRAVs oscillator strengths are similar (but weaker overall) to that of the absorption band associated with the charge excitation. The immense vibrational oscillator strength indicates that the added charges are 'easy to move', pointing to a relatively small effective kinetic mass, despite the relaxation energy associated with the added charges on the chain, namely the 'polaronic effect'.

A more complete picture of the DIA spectrum related with the added charges on the chains is shown in Fig. 4(a), where the DIA is displaced on a broader spectrum. It is seen that in fact the DIA spectrum of the charge excitations contain *two bands*, namely P1 peaked at ~0.4 eV and P2 with a peak at ~1.15 eV [41,42]. We therefore identify the charges on the copolymer chains as *polarons* since these excitations have two allowed absorption bands, as seen in many DIA and PIA spectra of homopolymers [33], and calculated for the copolymers [25]. From P1 band we

can extract the polaron relaxation energy in PTB7 copolymer upon doping to be ~ 0.3 eV (see Fig. 4(c) inset). This lower energy estimate takes into account the large dip superimposed on the P1 band at ~ 1600 cm^{-1} (or 0.2 eV). It is noteworthy that the appropriate sum of the polaron absorption energies according to Fig. 4(c) inset, namely 2E(P1)+E(P2)= 1.75 eV, which is the optical gap energy. This shows that the polaron energies are symmetrically located in the copolymer gap [33], as depicted in Fig. 4(c) inset. In addition, we also note that the relative strengths of the IRAVs to that of the two polaron bands is approximately 1:7. This indicates a reasonably small polaron kinetic effective mass, M_p that can be estimated using the AMM (see below).

A more detailed DIA spectrum of the vibrational modes shows that in fact some IRAVs do not reveal themselves as sharp absorption bands, but are in the form of dips (or ARs) superimposed onto the P1 DIA band of the polaron (see Fig. 4(b)) [28]. It is clearly seen that there are at least four large ARs in the DIA spectrum; and Fig. 3 shows that they grow upon iodine exposure. These ARs replace the traditional IRAVs that are formed upon doping in many π-conjugated homopolymers. Interestingly we note that there are no pronounced ARs in the lower frequency range below 1200 cm^{-1}. This indicates that the ARs are due to *interference* between the IRAVs and the polaron P1 band [28,43]. Since the polaron band in the DIA spectrum does not extend to frequencies smaller than 1200 cm^{-1}, there are no ARs that are formed below this frequency. In this case, we may consider the peak seen at ~1115 cm^{-1} as IRAV rather than AR, and take it into account in calculating the relative oscillation strengths of the vibration to that of the electronic absorption bands.

A detailed ARs spectrum is barely possible via DIA spectroscopy since doping increases inhomogeneity and disorder in the copolymer chains, which broadens the AR dips. A better ARs spectrum can be obtained via photogeneration. However, the photon absorption in the pristine copolymer does not usually lead to charge excitation, since the binding energy of the excitons is quite large (of order 0.4 eV [27]). An alternative way for polarons photogeneration is therefore in blend of the copolymer donor with fullerene acceptor molecules, such as PCBM. In this case, the photogenerated excitons in the copolymer may dissociate at the copolymer/fullerene interface, where an electron is donated to the fullerene acceptor and consequently a hole polaron is left on

the copolymer chains [6]. Under steady state conditions, hole polarons are photogenerated onto the copolymer chains in the same manner as doping with iodine, except that the disorder in the blend is less acute than that formed upon doping.

Figure 4(c) shows the PIA spectrum of PTB7/PCBM blend. The spectrum contains the two polaron bands P1 and P2, the related ARs, and another band at ~ 1.2 eV that was identified before as due to triplet excitons [41,42]. We checked that P1, P2 and ARs in the PIA spectrum have the same dependence on the laser excitation intensity and temperature, and therefore they originate from the same photoexcitation species, which we identify as photogenerated hole polarons on the PTB7 chains [41]. A more detailed PIA spectrum in the frequency range of the vibrational modes is shown in Fig. 4(d). At least five ARs can now be clearly identified, at frequencies slightly lower than those in the DIA spectrum of Fig. 4(b).

Analysis using the amplitude mode model

We now introduce the AMM for analyzing the strongly coupled vibrations that are revealed as peaks in the copolymer RRS spectrum and ARs in the DIA and PIA spectra, respectively. In previous applications of the AMM it has been explicitly assumed that the adiabatic approximation holds true [30]. This was a correct assumption since the Raman frequencies are much smaller than the electronic absorption bands. This approximation however does not hold in our case; since the vibrational frequencies are in resonance with the P1 polaron band. We thus need to use the modified AMM that includes non-adiabatic effects [28,43]. An important ingredient of the AMM is that all IRAVs are interconnected by being coupled to the same phonon propagator. The *bare* phonon propagator in the copolymer chain is given by [29]:

$$D_0(\omega) = \sum_n \frac{\lambda_n}{\lambda} \frac{(\omega_n^0)^2}{\omega^2 - (\omega_n^0)^2 - i\omega\delta_n}, \qquad (1)$$

where ω_n^0, δ_n, and λ_n are the bare frequencies, their natural width and electron-phonon (e-p) coupling constants; and $\sum\lambda_n=\lambda$ that is the total e-p coupling constant. The index, n varies from 1 to N, the number of coupled modes in the polymer chain; for example N=6 for PTB7 copolymer.

The bare frequencies in the coupled e-p chain are renormalized, since they interact with the electronic gap, so that their modified propagator is given by a 'Dyson-type' equation [32]:

$$D(\omega) = \frac{D_0(\omega)}{1 + (1 - 2\lambda^*)D_0(\omega)}\,, \qquad (2)$$

where the renormalization parameter, $2\lambda^*=(1-2\lambda E''(2\Delta_0))$, E'' is the second derivative of the total electron-phonon system vs. the dimerization amplitude, Δ, and $2\Delta_0$ is the dimerization gap at equilibrium [30]. The poles of Eq. (2) are the renormalized Raman frequencies, ω_n^R of the copolymer, given by the relation [32]:

$$D_0(\omega) = -(1 - 2\lambda^*)^{-1}, \qquad (3)$$

The renormalized AR frequencies, $\omega_{n,AR}$ appear as zeroes in the conductivity response, σ(ω) [28,43]:

$$\sigma(\omega) \sim \frac{1 + D_0(\omega)(1 - \alpha')}{1 + D_0(\omega)[1 + \mathrm{c1} - \alpha]}\,, \qquad (4)$$

which are given by the relation:

$$D_0(\omega) = -(1 - \alpha')^{-1}\,, \qquad (5)$$

Where α' is a non-adiabatic renormalization parameter. It is noteworthy that α' need not be the same for the ARs in PIA and DIA spectra, since the polaron excitation in PIA is 'free', whereas the polaron excitation in DIA is bound to the dopant molecule [28]. In contrast, the IRAV frequencies appear as poles in Eq. (4), given by the relation $D_0(\omega) = -[1+\mathrm{c1}-\alpha]^{-1}$ (where c1 and α are constants), which are practically suppressed by their proximity to the ARs.

When plotting the function $D_0(\omega)$ (Fig. 5(b)), we note that it has poles at the bare frequencies, ω_n^0 and approaches the value (-1) at low ω. This is because at ω=0 the numerator and denominator in $D_0(\omega)$ cancel each other, and $\sum$-λ_n/λ= -1. Equations (3) and (4) are in fact polynomial of order N in ω^2, and thus it is much easier to solve for the renormalized vibrational mode

frequencies by drawing a horizontal line at different values that correspond to the parameters λ^* or α'(see Fig. 5(b)). To fit the various renormalized frequencies using the AMM we have to find 2N-1 parameters associated with $D_0(\omega)$, and three additional parameters, namely λ^* and two different α' . This has been a formidable task; but when considering also the RRS intensities, it has made it much easier (see below).

The best fitting function $D_0(\omega)$ that describes the six most strongly coupled vibrations in PTB7 is shown in Fig. 5(b), together with three horizontal lines that represent the cases of RRS, PIA and DIA (Eqs. (3) and (5)). The fitting parameters for the best $D_0(\omega)$ are given in Table I. The fit with the experimental frequencies is excellent. We therefore conclude that the AMM is a good basic model for describing the strongly coupled vibrations in PTB7. We found that, in general $2\lambda^* > \alpha'$, and α'(DIA)> α'(PIA); this agrees with other polymers, where α' is in fact α(pinning) upon doping or photogeneration [28]. It is interesting to note that the horizontal line that describes the ARs in the DIA spectrum in fact has an intersection at ~ 1180 cm^{-1}; alas, there is no AR dip that is obtained at this frequency. The reason for the apparent 'failure' to form AR dip at that frequency is that the polaron DIA band does not extend to such low frequency; and hence interference with the amplitude mode #1 does not occur. Instead of an AR, the amplitude mode #1 appears in the DIA as a renormalized IRAV at 1115 cm^{-1} (denoted by a (*) in Fig. 5 panels (b) and (c)) that can be generated from the phonon propagator at a different α'.

One of the benefits of using the AMM to describe the most coupled vibrations of the copolymer chain is that it can predict the relative scattering intensities in the RRS spectrum [29]; this is a unique virtue, since, in general, this is rather impossible to predict. The reason behind this extraordinary ability is that all renormalized modes are related to each other through the same phonon propagator, which is not the case in RRS spectra of most compounds. It turns out that the Raman scattering intensity, I_n of each renormalized mode is inversely proportional to the slope of $D_0(\omega)$ at the renormalized frequencies [29]; namely $I_n \sim |dD_0(\omega)/d\omega|$ at $\omega=\omega_n^R$. Since the function $D_0(\omega)$ is known for PTB7 and we also found the proper parameter $2\lambda^*$ (=0.73) that describes the RRS frequencies, it is straightforward to calculate the RRS spectrum based on the AMM. This is nicely shown in Fig. 6, where the calculated RRS spectrum is compared to the experimental

spectrum. The fit is *superb*; and this validates the conclusion that the AMM is a reliable theoretical model for the vibrational frequencies in PTB7, and probably for many other D-A copolymers.

Another benefit of using the AMM for the vibrations in the class of the π-conjugated polymers is the ability to estimate the polaronic effective kinetic mass, M_p from the intensity ratio of the IRAVs to that of the electronic absorption bands. This is given by the following relation [31,32]:

$$\frac{M_p}{m^*} = \frac{\pi}{5.6}\frac{I_p}{I_v}\left(\frac{\Omega_1}{\Omega_0}\right)^2 , \qquad (6)$$

where I_p/I_v is the ratio of the polaronic absorption band, I_p to that of the IRAV I_v, m^* is the electron effective mass (~0.1 m_e in π-conjugated polymers) and the frequencies Ω_1 and Ω_0 are given by the relations [30]:

$$\Omega_0^{-2} = \sum_n \frac{\lambda_n}{\lambda}(\omega_n^0)^{-2} , \; \Omega_1^2 = \sum_n \frac{\lambda_n}{\lambda}(\omega_n^0)^2 , \qquad (7)$$

We obtain from the DIA spectrum shown in Fig. 4(b) $I_p/I_v \approx 6.7$; and from the AMM parameters given in Table I we calculate $(\Omega_1/\Omega_0)^2 \approx 1$. Using Eq. (6) we therefore estimate $M_P/m^* \approx 3.8$ for the polaron effective kinetic mass in PTB7. This shows that the polaronic mass is enhanced over the electron effective mass, m^* by ~3.8, which is intermediately large indicating that the 'polaronic effect', namely the polaron relaxation energy in PTB7 is still large, in agreement with the P1 band in the PIA spectrum (Fig. 4(c)). It is interesting to compare the obtained polaronic mass in PTB7 ($M_P/m^* \approx 3.8$) to the soliton mass M_S in t-$(CH)_x$ ($M_S/m^* \approx 6$), which was estimated using the same method [29]; the smaller polaronic mass here indicates a larger carrier mobility in PTB7. In addition the polaronic mass enhancement that we obtained for doped PTB7 may explain the low hole mobility in its blend with PCBM, which was measured to be $2\text{x}10^{-4}$ cm^2/Vs [44] that limits its application in OPV solar cells. We thus conclude that better growth of the PTB7 film may lead to a more planar structure of the copolymer chains, which, in turn may also increase the OPV solar cell efficiency based on this copolymer.

In summary, we studied the most strongly coupled vibrations in the pristine D-A copolymer PTB7 using resonant Raman scattering and doping induced absorption spectra, and in PTB7/PCBM blend using the photoinduced absorption technique. The six Raman active modes are renormalized when charge polarons are added to the copolymer chains upon doping and photogeneration. They revealed themselves as anti-resonant dips superposed on the lower polaron absorption band. We have shown that the amplitude mode model well describes the vibrational modes in all three spectra with a single phonon propagator in which all six modes are coupled together. From the AMM parameters in PTB7 we calculated the polaronic mass enhancement for charge excitation in this compound. The estimation of the polaronic kinetic mass from the application of the AMM to the polaron vibration and electronic spectra may be an effective tool for studying the charge mobilities in π-conjugated D-A copolymers that are used in various forms for OPV applications.

Acknowledgements:

The work at the University of Utah was supported by the AFOSR under award number FA9550-16-1-0207 (E.L.; RRS and PIA spectroscopy); NSF-MRSEC program DMR 1121252 (SB; DIA spectroscopy, and help with the acquisition of the FTIR spectrometer); and in part with funding from the Space Exploration and Optical Solutions Technology Research Initiative Fund at the University of Arizona (S.R.V).

References

1. G. Yu, J. Gao, J. C. Hummelen, F. Wudl, and A. J. Heeger, Polymer photovoltaic cells: Enhanced efficiencies via a network of internal donor-acceptor heterojunctions, Science **270**, 1789 (1995).

2. C. Brabec, Organic photovoltaics: technology and market, Sol. Energy Mater. Sol. Cells **83**, 273 (2004).

3. J. Peet, J. Y. Kim, N. E. Coates, W. L. Ma, D. Moses, A. J. Heeger and G. C. Bazan, Efficiency enhancement in low-bandgap polymer solar cells by processing with alkane dithiols, Nat. Mater. **6**, 497 (2007).

4. L. M. Peter, Towards sustainable photovoltaics: the search for new materials, Philos. Trans. R. Soc. A **369**, 1840 (2011).

5. F. He and L. Yu, How Far Can Polymer Solar Cells Go? In Need of a Synergistic Approach, J. Phys. Chem. Lett. **2**, 3102 (2011).

6. W. Ma, C. Yang, X. Gong, K. Lee, and A. J. Heeger, Thermally Stable, Efficient Polymer Solar Cells with Nanoscale Control of the Interpenetrating Network Morphology, Adv. Funct. Mater. **15**, 1617 (2005).

7. N. Blouin, A. Michaud, and M. Leclerc, A Low-Bandgap Poly(2,7-Carbazole) Derivative for Use in High-Performance Solar Cells, Adv. Mater. **19**, 2295 (2007).

8. H.-Y. Chen, J. Hou, S. Zhang, Y. Liang, G. Yang, Y. Yang, L. Yu, Y. Wu, and G. Li, Polymer solar cells with enhanced open-circuit voltage and efficiency, Nat. Photonics **3**, 649 (2009).

9. Y. Zhang, S. K. Hau, H.-L. Yip, Y. Sun, O. Acton, and A. K.-Y. Jen, Efficient Polymer Solar Cells Based on the Copolymers of Benzodithiophene and Thienopyrroledione, Chem. Mater. **22**, 2696 (2010).

10. W. Chen, T. Xu, F. He, W. Wang, C. Wang, J. Strzalka, Y. Liu, J. Wen, D. J. Miller, J. Chen et al., Hierarchical nanomorphologies promote exciton dissociation in polymer/fullerene bulk heterojunction solar cells, Nano Lett. **11**, 3707 (2011).

11. H. Zhou, Y. Zhang, J. Seifter, S. D. Collins, C. Luo, G. C. Bazan, T.-Q. Nguyen, and A. J. Heeger, High-efficiency polymer solar cells enhanced by solvent treatment, Adv. Mater. **25**, 1646 (2013).

12. J. You, L. Dou, K. Yoshimura, T. Kato, K. Ohya, T. Moriarty, K. Emery, C.-C. Chen, J. Gao, G. Li, and Y.Yang, A polymer tandem solar cell with 10.6% power conversion efficiency, Nat. Commun. **4**, 1446 (2013).

13. L. Dou, J. You, Z. Hong, Z. Xu, G. Li, R. A. Street, and Y. Yang, 25th anniversary article: A decade of organic/polymeric Photovoltaic Research, Adv. Mater. **25**, 6642 (2013).

14. R. S. Kularatne, H. D. Magurudeniya, P. Sista, M. C . Biewer, and M. C. Stefan, Donor–acceptor semiconducting polymers for organic solar cells, J. Polym. Sci., Part A: Polym. Chem. **51**, 743 (2013).

15. S. A. Hawks, F. Deledalle, J. Yao, D. G. Rebois, G. Li, J. Nelson, Y. Yang, T. Kirchartz, and J. R. Durrant, Relating Recombination, Density of States, and Device Performance in an Efficient Polymer:Fullerene Organic Solar Cell Blend, Adv. Eng. Mater. **3**, 1201 (2013).

16. Y. Liu, J. Zhao, Z. Li, C. Mu, W. Ma, H. Hu, K. Jiang, H. Lin, H. Ade, and H. Yan, Aggregation and morphology control enables multiple cases of high-efficiency polymer solar cells, Nat. Commun. **5**, 5293 (2014).

17. Z. He, C. Zhong, S. Su, M. Xu, H. Wu and Y. Cao, Enhanced power-conversion efficiency in polymer solar cells using an inverted device structure, Nat. Photonics **6**, 593 (2012).

18. D. D. Nuzzo, C. Fontanesi, R. Jones, S. Allard, I. Dumsch, U. Scherf, E. von Hauff, S. Schumacher and E. D. Como, How intermolecular geometrical disorder affects the molecular doping of donor–acceptor copolymers, Nat. Commun. **6**, 6460 (2015).

19. C. Risko, M. D. McGehee, and J.-L. Bredas, A quantum-chemical perspective into low optical-gap polymers for highly-efficient organic solar cells, Chem. Sci. **2**, 1200 (2011).

20. N. Blouin, A. Michaud, D. Gendron, S. Wakim, E. Blair, R. Neagu-Plesu, M. Belletête, G. Durocher, Y. Tao and M. Leclerc, Toward a rational design of poly(2,7-carbazole) derivatives for solar cells, J. Am. Chem. Soc. **130**, 732 (2008).

21. B. P. Karsten, J. C. Bijleveld, L. Viani, J. Cornil, J. Gierschner, and R. A. J. Janssen, Electronic structure of small band gap oligomers based on cyclopentadithiophenes and acceptor units, J. Mater. Chem. **19**, 5343 (2009).

22. T. M. Pappenfus, J. A. Schmidt, R. E. Koehn, and J. D. Alia, PBC-DFT Applied to Donor-Acceptor Copolymers in Organic Solar Cells: Comparisons between Theoretical Methods and Experimental Data, Macromolecules **44**, 2354 (2011).

23. N. M. O'Boyle, C. M. Campbell, and G. R. Hutchison, Computational Design and Selection of Optimal Organic Photovoltaic Materials, J. Phys. Chem. C **115**, 16200 (2011).

24. N. Banerji, E. Gagnon, P.-Y. Morgantini, S. Valouch, A. R. Mohebbi, J.-H. Seo, M. Leclerc, and A. J. Heeger, Breaking Down the Problem: Optical Transitions, Electronic Structure, and Photoconductivity in Conjugated Polymer PCDTBT and in its Separate Building Blocks, J. Phys. Chem. C **116**, 11456 (2012).

25. C. Wiebeler, R. Tautz, J. Feldmann, E. von Hauff, E. D. Como, and S. Schumacher, Spectral signatures of polarons in conjugated co-polymers, J. Phys. Chem. B **117**, 4454 (2013).

26. R. Tautz, E. D. Como, T. Limmer, J. Feldmann, H.-J. Egelhaaf, E. von Hauff, V. Lemaur, D. Beljonne, S. Yilmaz, I. Dumsch et al., Structural correlations in the generation of polaron pairs in low-bandgap polymers for photovoltaics, Nat. Commun. **3**, 970 (2012).

27. K. Aryanpour, T. Dutta, U. N. V. Huynh, Z. V. Vardeny, and S. Mazumdar, Theory of Primary Photoexcitations in Donor-Acceptor Copolymers, Phys. Rev. Lett. **115**, 267401 (2015).

28. R. Österbacka, X. M. Jiang, C. P. An, B. Horovitz, and Z. V. Vardeny, Photoinduced Quantum Interference Antiresonances in π-Conjugated Polymers, Phys. Rev. Lett. **88**, 226401 (2002).

29. E. Ehrenfreund, Z. Vardeny, O. Brafman, and B. Horovitz, Amplitude and phase modes in trans-polyacetylene: Resonant Raman scattering and induced infrared activity, Phys. Rev. B **36**, 1535 (1987).

30. B. Horovitz, Infrared activity of Peierls systems and application to polyacetylene, Solid State Commun. **41**, 729 (1982).

31. Z. Vardeny, J. Orenstein, and G. L. Baker, Photoinduced Infrared Activity in Polyacetylene, Phys. Rev. Lett. **50**, 2032 (1983).

32. Z. Vardeny, E. Ehrenfreund, O. Brafman, and B. Horovitz, Resonant Raman Scattering from Amplitude Modes in trans-$(CH)_x$ and -$(CD)_x$, Phys. Rev. Lett. **51**, 2326 (1983).

33. R. Österbacka, C. P. An, X. M. Jiang, and Z. V. Vardeny, Two-Dimensional Electronic Excitations in Self-Assembled Conjugated Polymer Nanocrystals, Science **287**, 839 (2000).

34. Y. Liang, Z. Xu, J. Xia, S.-T. Tsai, Y. Wu, G. Li, C. Ray, and L. Yu, For the bright future-bulk heterojunction polymer solar cells with power conversion efficiency of 7.4%, Adv. Mater. **22**, 135 (2010).

35. W. Chen, T. Xu, F. He, W. Wang, C. Wang, J. Strzalka, Y. Liu, J. Wen, D. J. Miller, J. Chen, K. Hong, L. Yu, and S. B. Darling, Hierarchical nanomorphologies promote exciton dissociation in polymer/fullerene bulk heterojunction solar cells, Nano Lett. **11**, 3707 (2011).

36. Y. W. Soon, H. Cho, J. Low, H. Bronstein, I. McCulloch, and J. R. Durrant, Correlating triplet yield, singlet oxygen generation and photochemical stability in polymer/fullerene blend films, Chem. Commun. **49**, 1291 (2013).

37. J. Razzell-Hollis, J. Wade, W. C. Tsoi, Y. Soon, J. Durrant, and J.-S. Kim, Photochemical stability of high efficiency PTB7:$PC_{70}BM$ solar cell blends, J. Mater. Chem. A **2**, 20189 (2014).

38. T. Drori, J. Holt, and Z. V. Vardeny, Optical studies of the charge transfer complex in polythiophene/fullerene blends for organic photovoltaic applications, Phys. Rev. B 82, 075207 (2010).

39. G. Grancini, M. Maiuri, D. Fazzi, A. Petrozza, H.-J. Egelhaaf, D. Brida, G. Cerullo, and G. Lanzani, Hot exciton dissociation in polymer solar cells, Nat. Mater. **12**, 29 (2013).

40. D. Fazzi, G. Grancini, M. Maiuri, D. Brida, G. Cerullo, and G. Lanzani, Ultrafast internal conversion in a low band gap polymer for photovoltaics: experimental and theoretical study, Phys. Chem. Chem. Phys. **14**, 6367 (2012).

41. T. Basel, U. Huynh, T. Zheng, T. Xu, L. Yu, and Z. V. Vardeny, Optical, Electrical, and Magnetic Studies of Organic Solar Cells Based on Low Bandgap Copolymer with Spin ½ Radical Additives, Adv. Funct. Mater. **25**, 1895 (2015).

42. B. R. Gautam, T. D. Nguyen, E. Ehrenfreund, and Z. V. Vardeny, Magnetic field effect on excited-state spectroscopies of π-conjugated polymer films, Phys. Rev. B **85**, 205207 (2012).

43. B. Horovitz, R. Österbacka, and Z.V. Vardeny, Multiple Fano effect in charge density wave systems, Synthetic Metals **141**, 179 (2004).

44. B. Ebenhoch, S.A.J. Thomson, K. Genevicius, G. Juška, and I.D.W. Samuel, Charge carrier mobility of the organic photovoltaic materials PTB7 and $PC_{71}BM$ and its influence on device performance, Organic Electronics **22**, 62 (2015).

Figure Captions

FIG. 1. (a) The backbone structure of the D-A copolymer that contains two different moieties. (b) The photoluminescence and absorption spectra of PTB7 film at ambient conditions.

FIG. 2. The Raman scattering (a) and IR-absorption spectra (b) of PTB7 film measured at ambient conditions. The most strongly coupled modes 1 to 6 are assigned. The (*) symbol denotes impurity-related mode [37].

FIG. 3. The evolution of the doping induced absorption of PTB7 film upon exposure to iodine vapor at various time durations as given. The P1 polaron band and related IRAVs are assigned.

FIG. 4. The doping induced absorption (DIA) spectra of PTB7 film (a) and (b), and photoinduced absorption (PIA) spectra of PTB7/PCBM blend film (c) and (d). The polaron bands P1 and P2 are assigned (see inset in panel (c)); the triplet PIA band, T is also denoted in (c). The IRAVs are shown in more detail in panels (b) and (d), where the anti-resonances (ARs) are denoted with arrows pointing to dips superimposed on the polaron P1 band.

FIG. 5. The measured spectrum (lines) and calculated vibrational mode frequencies (symbols) in PTB7 film for (a) photoinduced absorption (PIA); (c) doping-induced absorption (DIA); and (d) resonant Raman scattering. The 'bare' phonon propagator, $D_0(\omega)$ is shown in (b), where the horizontal lines are obtained using $2\lambda^*$=0.73 (RRS, down triangles), α'(PIA)=0.44 (ARs, circles), and α'(DIA)=0.44 (ARs, up triangles). The modes 1 to 6 are assigned. $D_0(\omega)$ parameters are given in Table I. The (*) symbol in panels ((b) and (c) denotes an IRAV at 1115 cm^{-1}, that is not an AR dip (see text for discussion).

FIG. 6. The RRS spectrum of PTB7 as measured (a) and calculated (b) using the AMM parameters given in Table I.

Table I

The best fitting parameters for the bare phonon propagator, $D_0(\omega)$ that describes the six most strongly coupled vibrational modes in PTB7. ω_n^0 are the bare frequencies, λ_n/λ are their relative e-p coupling, and δ_n are their natural width used to fit the RRS spectrum (Fig. 6(b)).

Mode index	ω_n^0 (bare frequency) cm^{-1}	λ_n/λ	δ_n (RRS) cm^{-1}
1	1240	0.005	9
2	1316	0.002	10
3	1445	0.008	25
4	1520	0.03	60
5	1575	0.002	13
6	1760	0.953	20

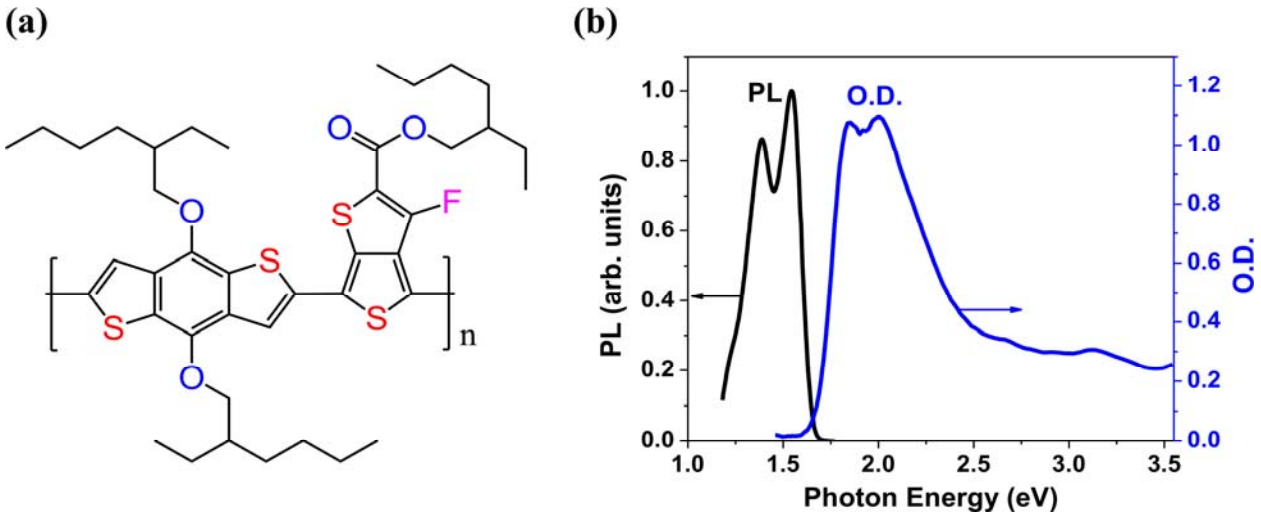

FIG. 1. (a) The backbone structure of the D-A copolymer that contains two different moieties. (b) The photoluminescence and absorption spectra of PTB7 film at ambient conditions.

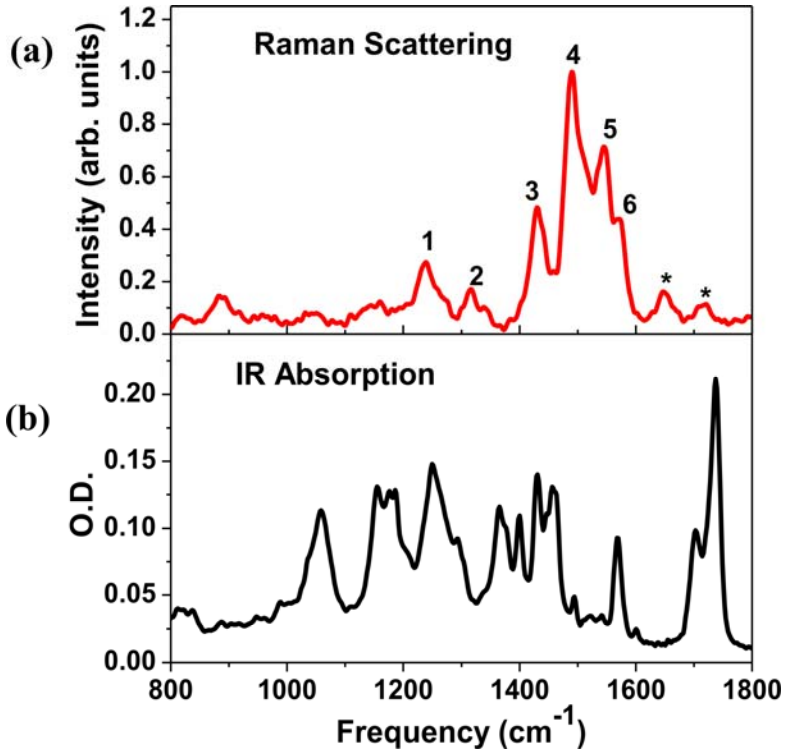

FIG. 2. The Raman scattering (a) and IR-absorption spectra (b) of PTB7 film measured at ambient conditions. The most strongly coupled modes 1 to 6 are assigned. The (*) symbol denotes impurity-related modes [37]

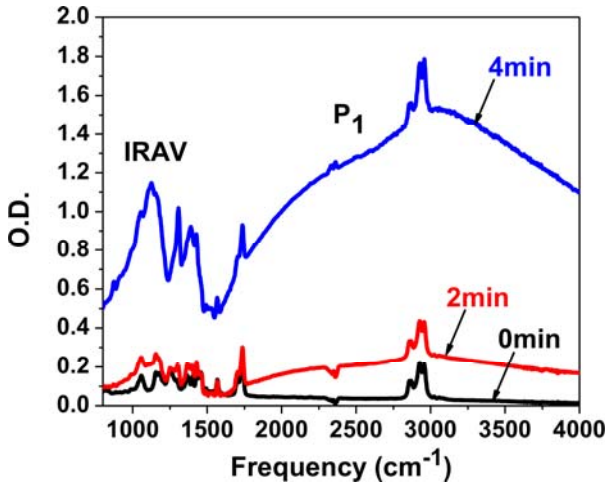

FIG. 3. The evolution of the doping induced absorption of PTB7 film upon exposure to iodine vapor at various time durations as given. The P1 polaron band and related IRAVs are assigned.

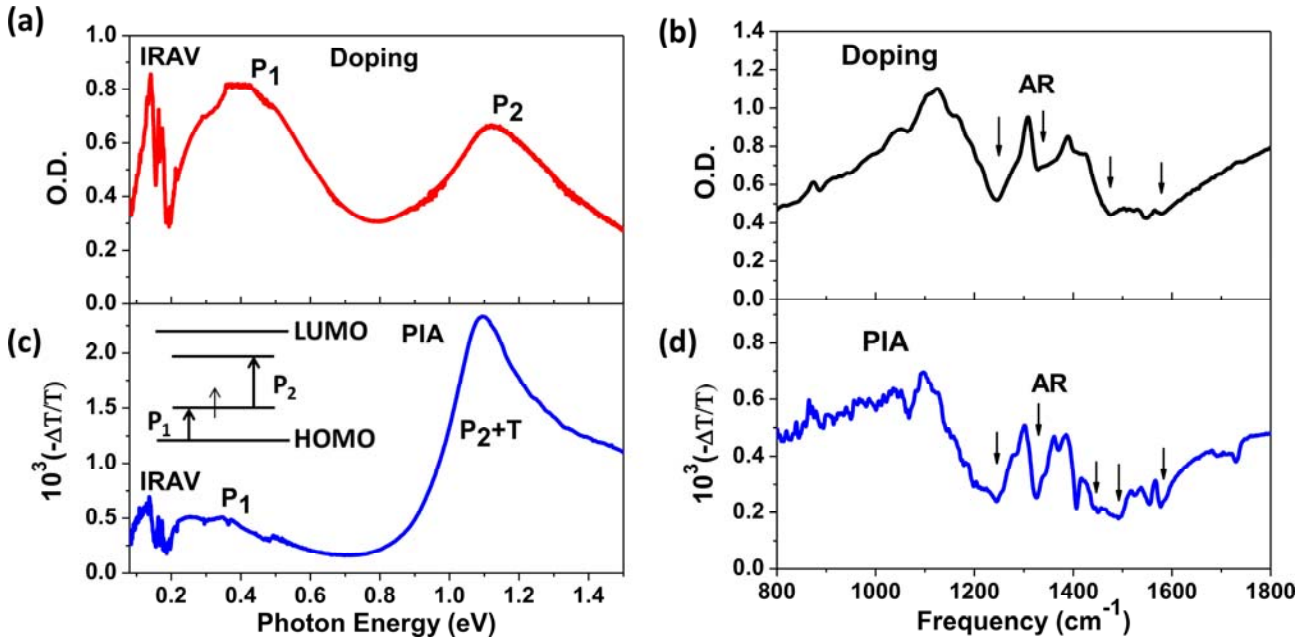

FIG. 4. The doping induced absorption (DIA) (a) and (b), and photoinduced absorption (PIA) spectra (c) and (d) of PTB7/PCBM blend film. The polaron bands P1 and P2 are assigned (see inset in panel (c)); the triplet PIA band, T is also denoted in (c). The IRAVs are shown in more detail in panels (b) and (d), where the anti-resonances (ARs) are denoted with arrows pointing to dips superimposed on the polaron P1 band.

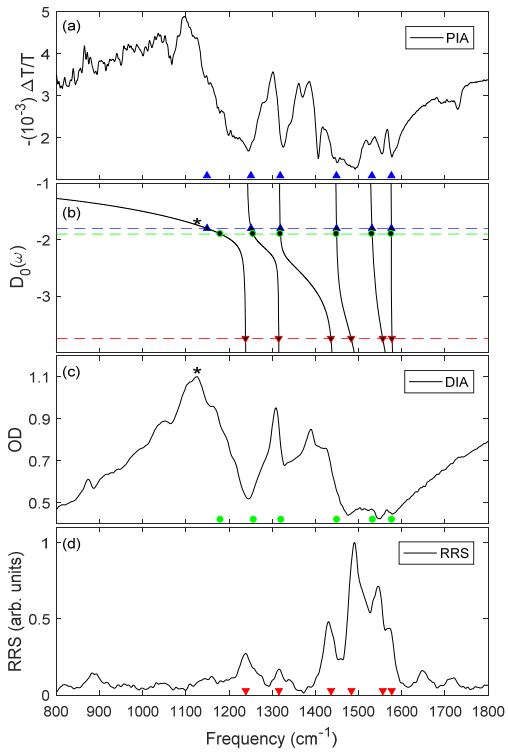

FIG. 5. The measured spectrum (lines) and calculated vibrational mode frequencies (symbols) in PTB7 film for (a) photoinduced absorption (PIA); (c) doping-induced absorption (DIA); and (d) resonant Raman scattering. The 'bare' phonon propagator, $D_0(\omega)$ is shown in (b), where the horizontal lines are obtained using $2\lambda^*=0.73$ (RRS, down triangles), α'(PIA)=0.44 (ARs, circles), and α'(DIA)=0.44 (ARs, up triangles). The modes 1 to 6 are assigned. $D_0(\omega)$ parameters are given in Table I. The (*) symbol in panels ((b) and (c) denotes an IRAV at 1115 cm^{-1}, that is not an AR dip (see text for discussion).

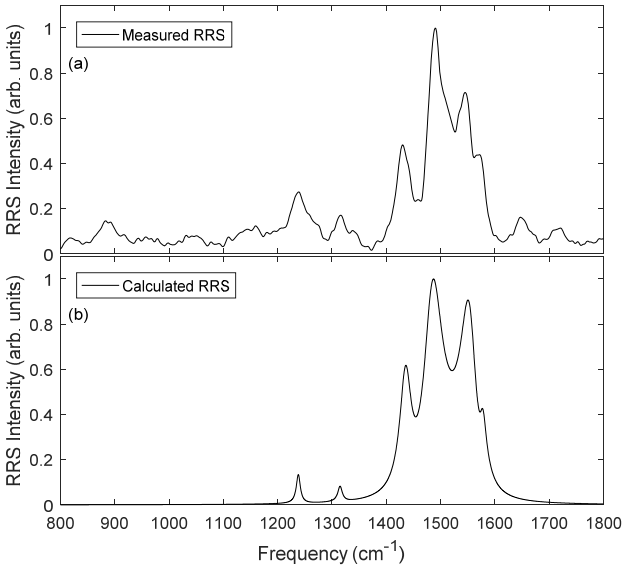

FIG. 6. The RRS spectrum of PTB7 as measured (a) and calculated (b) using the AMM parameters given in Table I.